



1 Gap-Filling of Turbulent Heat Fluxes over Rice–Wheat-Rotation 2 Croplands Using the Random Forest Model

3 Jianbin Zhang¹, Zexia Duan¹, Shaohui Zhou¹, Yubin Li¹, Zhiqiu Gao¹

4 ¹ School of Atmospheric Physics, Nanjing University of Information Science & Technology, Nanjing, 210044, China

5 *Correspondence to:* Dr. Yubin Li (liyubin@nuist.edu.cn)

6 **Abstract.** This study investigated the accuracy of the Random Forest (RF) model in gap-filling the sensible (H) and latent heat
7 (LE) fluxes, by using the observation data collected at a site over rice–wheat-rotation croplands in Shouxian County of eastern
8 China from 15 July 2015 to 24 April 2019. Firstly, the variable significances of the machine learning (ML) model’s five input
9 variables, including the net radiation (Rn), winds speed (WS), temperature (T), relative humidity (RH), and air pressure (P),
10 were examined, and it was found that Rn accounted for 78% and 76% of the total variable significance in H and LE calculating,
11 respectively, showing that it was the most important input variable. Secondly, the RF model’s accuracy with the five-variable
12 (Rn, WS, T, RH, P) input combination was evaluated, and the results showed that the RF model could reliably gap-fill the H
13 and LE with mean absolute errors (MAEs) of 5.88 Wm⁻² and 20.97 Wm⁻², and root mean square errors (RMSEs) of 10.67 Wm⁻²
14 and 29.46 Wm⁻², respectively. Thirdly, 4-variable input combinations were tested, and it was found that the best input
15 combination was (Rn, WS, T, P) with the MAE of H and LE reduced by 12.65% and 7.12%, respectively, after removing RH
16 from the input list. At last, through the Taylor diagram, H and LE gap-filling accuracy of the RF model, the support vector
17 machine (SVM) model, the k-nearest neighbor (KNN) model, and the gradient boosting decision tree (GBDT) model was
18 inter-compared, and the statistical metrics showed that RF was the most accurate for both H and LE gap-filling, while the LR
19 and KNN model performed the worst for H and LE gap-filling, respectively.

20

21 1 Introduction

22 The turbulent fluxes between the atmosphere and the ground play a crucial role in global climate change and atmospheric
23 circulation, and the inaccuracy of long-term observations of surface turbulent fluxes is a major factor in erroneous weather
24 predictions and climate projections. Research on the ecological effects of urban green spaces, agricultural ecosystems, and
25 forests all use surface turbulent fluxes as key indicators. Currently, the eddy covariance (EC) technique can be used to directly
26 measure the turbulent fluxes (Wilson et al., 2001; Jiang et al., 2021; Wang et al., 2021). However, due to sensor failure and
27 adverse meteorological factors (such as rainfall and frost), these high-frequency turbulence data are subject to errors (Khan et
28 al., 2018). As a result, it is difficult to obtain a continuous time series of ground-based turbulent fluxes. Furthermore, quality
29 assurance methods lead to unavailable sections of flux datasets (Nisa et al., 2021). Based on the above reasons, gap-filling is
30 in need to retrieve continuous datasets of EC-based fluxes. Researchers have developed approaches based on existing



31 meteorological information to fill up the gaps in atmospheric databases, such as interpolation, nonlinear regression, mean
32 diurnal method, and sampling techniques from the marginal distribution (Falge et al., 2001; Hui et al., 2004; Stauch et al.,
33 2006; Foltnov et al., 2020). Further, the ML technique has also become an effective method to be used in the calculation of
34 turbulent fluxes (McCandless et al., 2022).

35

36 As a result of recent developments in high computing technology, machine-learning-based algorithms have been developed
37 and successfully used in various areas, such as natural language processing, data mining, biometrics, computer vision, search
38 engines, clinical applications, video games, robots, etc. To address the missing data issue, machine-learning-based models
39 have recently been used to fill data gaps in meteorological elements and turbulent fluxes (Bianco et al., 2019; Yu et al., 2020).
40 As a result of their reliable and repeatable results, these models are now regarded as a standard gap-filling algorithm (Beringer
41 et al., 2017; Isaac et al., 2017). ML algorithms have several deficiencies even if they perform well in some areas. For instance,
42 over-fitting is a major concern that can occur when the training window is too short or the training dataset's quality is poor.
43 That's because the present ML approaches are not sufficiently adaptable to work in extreme situations with large values
44 (Kunwor et al., 2017; Moffat et al., 2007). Furthermore, even with the best technique, the model uncertainty of gap-filling still
45 plays a role, particularly when the gaps are relatively large. Numerous novel ML and optimization algorithms have been created
46 and put to use in numerous scientific domains since the 2000s, and their superiority has been demonstrated, either singly or as
47 a component of a hybrid or ensemble model (e.g. Gani et al., 2016).

48

49 Based on the need for fluxes dataset gap-filling, and the effectivity of the ML technique, this paper aims to, firstly, investigate
50 the performance of the RF machine learning algorithm trained from a dataset obtained over rice-wheat-rotation croplands in
51 Shouxian County, eastern China, in gap-filling the sensible and latent heat fluxes; and secondly, to analyze the RF model's
52 accuracy with various meteorological input combinations during training; and thirdly, to compare the performance of RF model
53 with other four typical ML models.

54

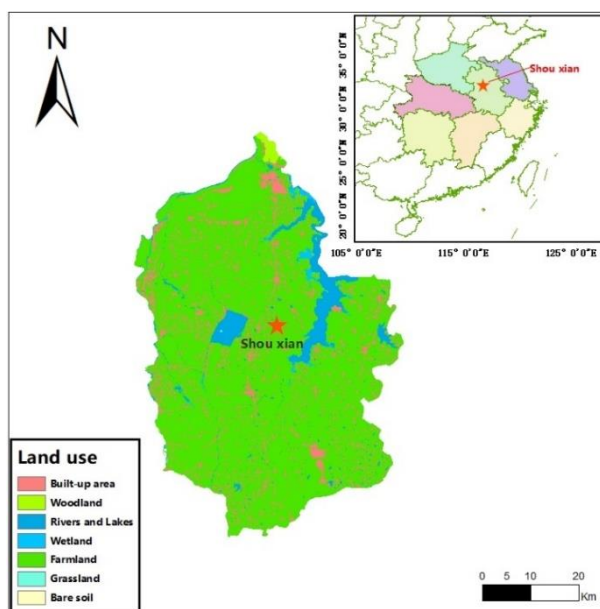
55 **2 Materials and Methods**

56 **2.1 Study area**

57 This observation was conducted at a site in Shouxian County in the eastern Chinese province of Anhui (32.42 °N, 116.76 °E)
58 (Figure 1). The altitude of the site is 27 meters, and the annual mean air temperature and annual cumulative precipitation here
59 are 16 °C and 1115 mm, respectively. This observation site is rather flat, with farmland accounting for more than 90% of the
60 area. Winter wheat is grown here from November until late May, while from June to November the field is flooded, plowed,
61 and harrowed as rice paddies (Duan et al., 2021) (Figure 2). The subtropical northern boundary of the monsoon humid climatic
62 type describes the area's climate.



63



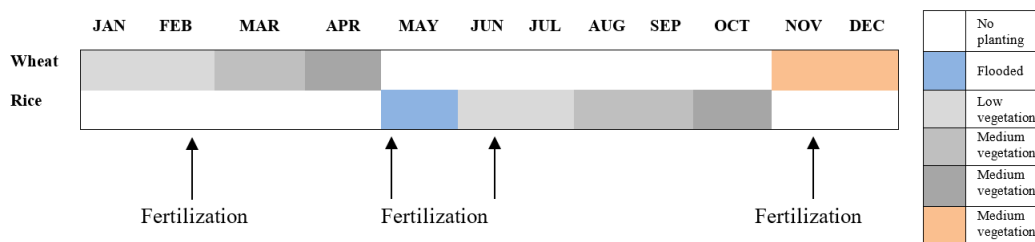
64

65

66

Figure 1. Geographical location and land-cover map of Shouxian County.

67



68

69

70

Figure 2. Crop calendars for the rice and wheat in the North Yangtze River Delta region.

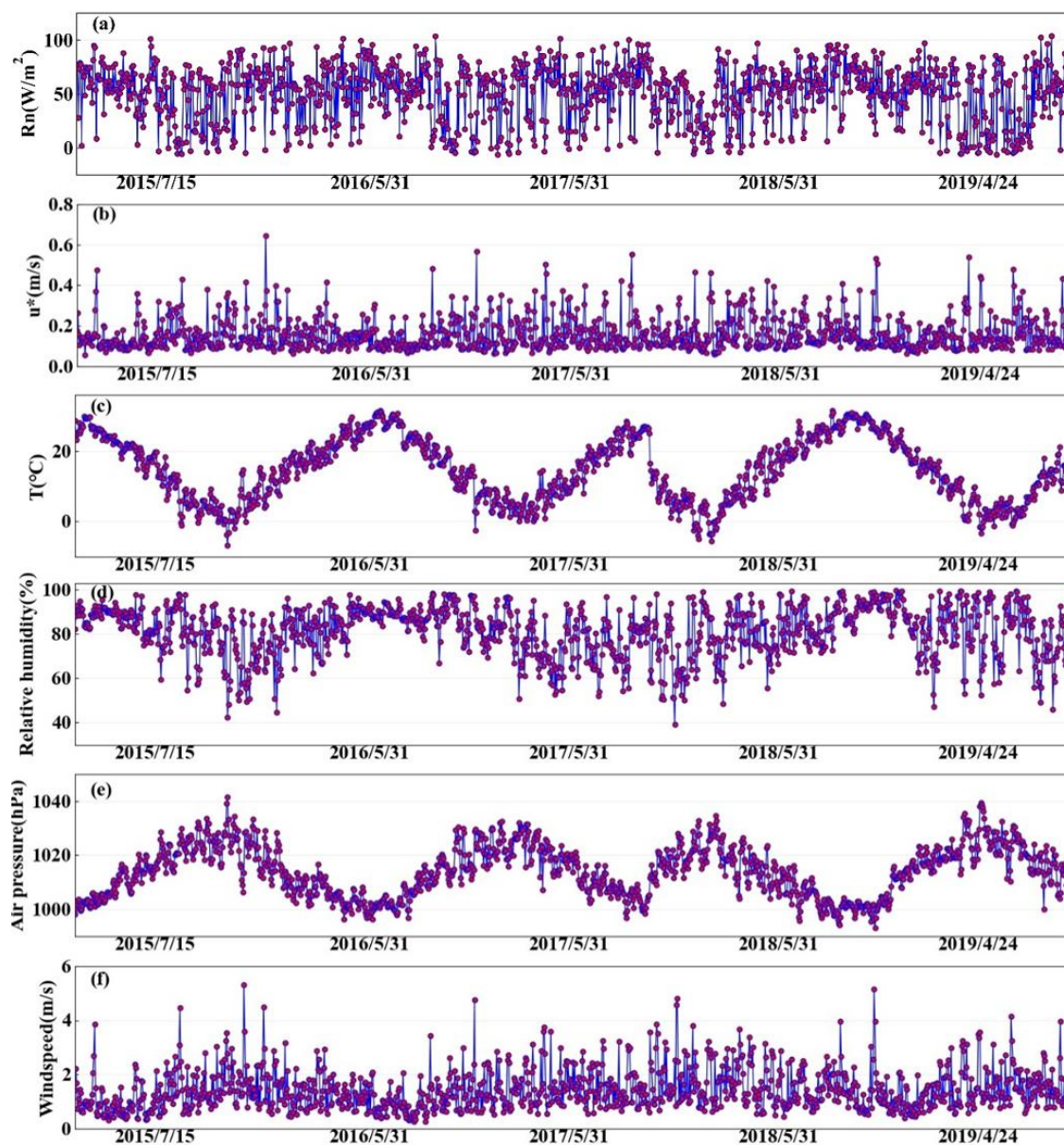
71

72 2.2 Data

73 Over the site described above, EC sensors (EC 150, Campbell Scientific Inc., Logan, UT, USA) were installed at 2.5 meters
 74 above the ground, including a three-dimensional sonic anemometer (CSAT3, Campbell Scientific Inc., Logan, UT, USA) and
 75 a CO₂/H₂O open-path infrared gas analyzer. The sensible and latent heat fluxes were computed half-hourly using EddyPro
 76 software, with time lag compensation, double coordinate rotation, spectrum correction, and Webb-Pearman-Leuning density



77 correction (Wutzler et al., 2018; Anapalli et al., 2019). Poor-quality fluxes (Eddypro quality check flag value=2) were
78 discarded. And a quality check based on the relationship between the measured flux and friction velocity was carried out to



79
80
81
82
83

Figure 3. Daily averaged a) Rn: net radiation(Wm^{-2}), b) u^* : friction velocity(m/s), c) T: air temperature($^{\circ}\text{C}$), d) RH: relative humidity(%), e) P: air pressure(hPa), and f) WS: wind speed(m s^{-1}).



84 remove the biased data (Papale et al., 2006). Then, using the marginal distribution sampling technique, the flow data were gap-
85 filled (Reichstein et al., 2005). The time series of air temperature, relative humidity, wind speed, air pressure, friction velocity,
86 and net radiation were also subjected to quality control. According to the criteria of $X(h) < (X - 4\sigma)$ or $X(h) > (X + 4\sigma)$, where
87 $X(h)$ indicates the time series of the component, X is the mean across the averaging interval, and σ is the standard deviation,
88 noisy data were eliminated (Gao et al., 2003). Data observed from 15 July 2015 to 24 April 2019 are used in this study, and
89 Figure 3 shows the daily average data of R_n : net radiation($W m^{-2}$), u^* : friction velocity(m/s), T : air temperature($^{\circ}C$), RH :
90 relative humidity(%), P : air pressure(hPa), and WS : wind speed($m s^{-1}$).

91

92 2.3 The RF Model

93 RF is a machine learning method that is quick, adaptable, and frequently used to analyze classification and regression jobs
94 (Breiman, 2001). This model can successfully evaluate highly dimensional and multicollinear data and is resistant to overfitting
95 (Belgiu et al., 2016). The RF model provides a feature-selection tool to assist in determining the importance of the predictor.
96 The contribution of each variable to the model, with important variables having a higher effect on the results of the model
97 evaluation, is the definition of feature significance (Liu et al., 2021). 90% of the data collected at the Shouxian observation
98 site throughout the study period were used to train the RF model, while the remaining 10% was used to independently validate
99 the model (hereafter, validation dataset). To lessen the overfitting in this case, a 10-fold cross-validation (CV) procedure was
100 used (Cai et al., 2020). All training data used here was randomly divided into ten subsamples of equal size for the 10-fold CV
101 tests. And nine out of the ten subsamples were used as training data (hereafter, training dataset), while the remaining subsample
102 was used as testing data (hereafter, testing dataset). All ten of the subsamples were utilized as testing data exactly once for
103 each of the 10 iterations of the CV procedure. One estimate was created by averaging the 10 findings from the folds. We
104 modified the four RF model hyperparameters based on Bayesian optimization to get the optimal model (Baareh et al., 2021;
105 Frazier, P.I., 2018): the maximum number of features considered to split a node (Max features), the maximum number of trees
106 to build (n estimators), the minimum sample number placed in a node prior to the node being split (min split), and the maximum
107 number of levels for each decision tree (Max depth). The simulated performance of the 10-fold CV outcomes was evaluated
108 using four statistical metrics: the correlation coefficient (r), mean absolute error (MAE), root mean square error (RMSE), and
109 standard deviation(σ_n). As a result, the final RF model's parameters were adjusted to n estimators = 246, min split = 2, Max
110 features = 10, and Max depth = 35, to have the best statistical metrics.

111 The four statistical metrics are calculated by:

112

$$r = \frac{\sum_{i=1}^N (S_i - \bar{S})(O_i - \bar{O})}{\sqrt{\sum_{i=1}^N (S_i - \bar{S})^2} \sqrt{\sum_{i=1}^N (O_i - \bar{O})^2}} \quad (1)$$

113

114

$$MAE = \frac{1}{N} \sum_{i=1}^N |S_i - O_i| \quad (2)$$



115

116

$$\text{RMSE} = \sqrt{\frac{\sum_{i=1}^N (S_i - O_i)^2}{N}}, \quad (3)$$

117

118

$$\sigma_n = \frac{\sqrt{\sum_{i=1}^N (S_i - O_i)^2}}{N}. \quad (4)$$

119

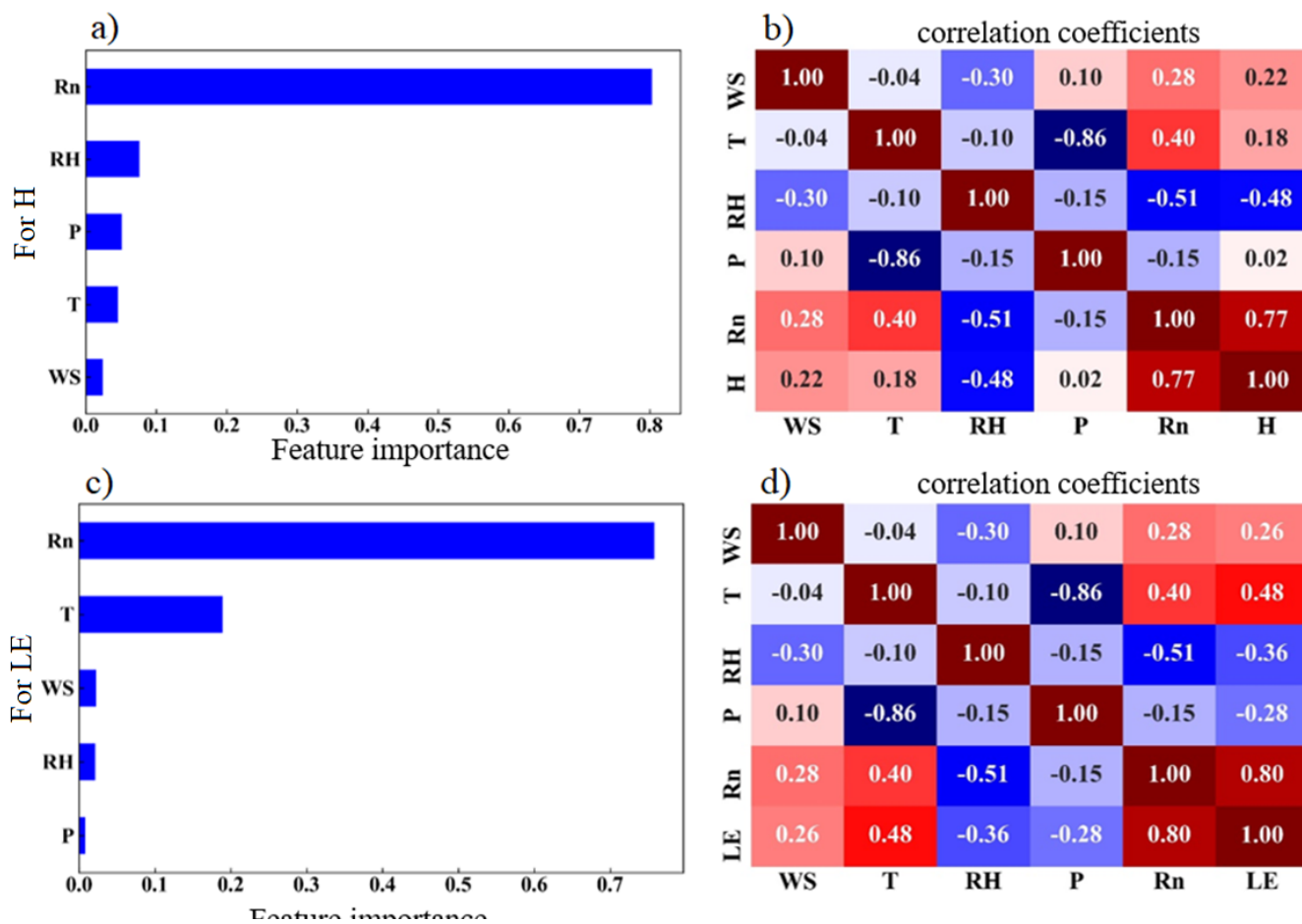
120 where S stands for the modeled value, O is the observation, \bar{O} is the mean observed value, and \bar{S} is the mean modeled
121 observation, σ_n indicates the standard deviation. The subscript i represents the serial number of samples, and N represents the
122 total number of samples.

123

124 3 Results and discussion

125 3.1 Driving Factors of H and LE on a Seasonal Scale

126 The possible driving factors of H and LE were investigated to determine their respective contributions by the RF model as
127 shown in Figure 4. Rn, which accounted for 78% and 76% of the total variable significance of H and LE, respectively, was the
128 most crucial variable in regulating the heat fluxes (Figures 4a and 4c). Consistent with the high variable significance values,
129 H and LE also had the highest r of 0.79 and 0.75 with H and LE, respectively, as shown in Figures 4b and 4d. The other four
130 factors contributed much smaller than Rn, and WS, T, RH, and P had importance values of 2%, 4%, 7%, and 5% (2.2%, 19%,
131 2%, and 0.6%) for H (LE), respectively. In general, all of these predictors played a role in the H and LE calculation, and for
132 H, the sequence of importance was Rn, RH, P, T, and WS; while for LE, it was Rn, T, WS, RH, and P. The most significant
133 impact on the change of H and LE came from Rn, which was the most important energy source of the surface and modulated
134 the surface temperature directly. The WS, T, and RH also affected H and LE according to the Monin-Obukhov similarity
135 theory (Monin and Obukhov, 1954), while P represented the contributions from the background weather systems.



136

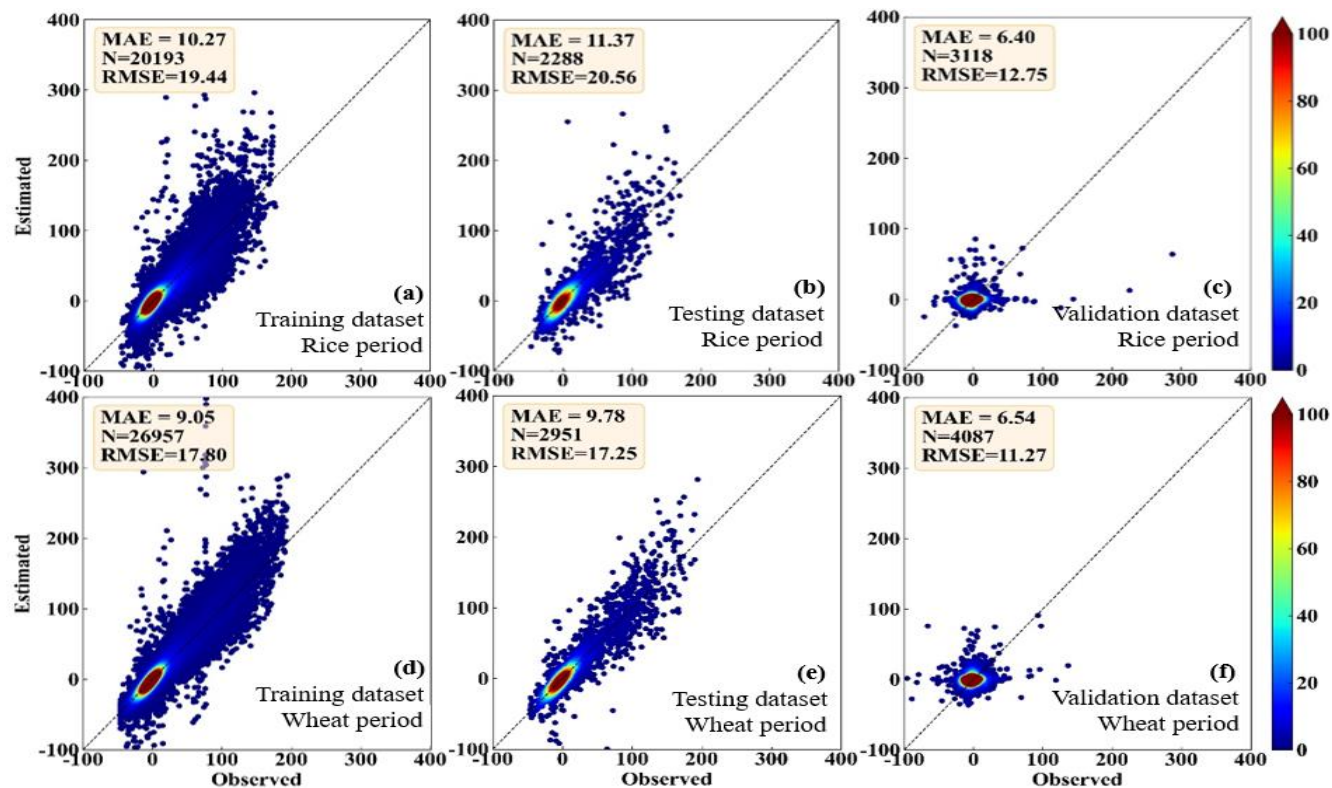
137 **Figure 4.** The feature importance of the variables for a) H and c) LE, and the correlation coefficient between each of the input
 138 variables for b) H and d) LE.
 139

140 **3.2 RF Model Evaluation**

141 Figures 5-6 show the comparison between the observed and the RF-estimated H and LE, respectively. In the period of rice, the
 142 RF model showed good performance for both the training dataset (MAE = 8.51 and 17.89 Wm⁻²; RMSE = 14.11 and 29.82 Wm⁻²
 143 ², for H and LE, respectively) and the testing dataset (MAE = 9.61 and 10.34 Wm⁻², RMSE = 15.63 and 17.21 Wm⁻², for H and
 144 LE, respectively) (Figures 5a, 5b, 6a, and 6b). RF model also showed high consistency with direct measurements for the
 145 validation dataset (MAE = 5.88 and 20.97 Wm⁻², RMSE = 10.67 and 29.46 Wm⁻², for H and LE, respectively), (Figures 5c and
 146 6c). In the period of wheat, the performance of the RF model for the training, testing, and validation datasets of H and LE was
 147 similar to that in the period of rice. For the training, testing, and validation datasets, respectively, the MAEs are 7.18, 8.01,
 148 and 6.01 Wm⁻² for H, and 13.58, 8.82, and 19.93 Wm⁻² for LE; and the RMSEs are 12.27, 13.61, and 9.86 Wm⁻² for H, and



149 24.92, 15.17, and 28.74 Wm^{-2} for LE (Figure 5d,e,f, Figure 6 d,e,f). These results demonstrate that the RF model is capable of
150 effectively calculating the H and LE with input variables of Rn, WS, T, RH, and P.



151
152
153
154
155
156

Figure 5. Scatter density plots of the observed and the RF-estimated H values, a) and d) for the training dataset, b) and e) for the testing dataset, and c) and f) for the validation dataset. And a), b) and c) are in the period of rice, while d), e) and f) are in the period of wheat.

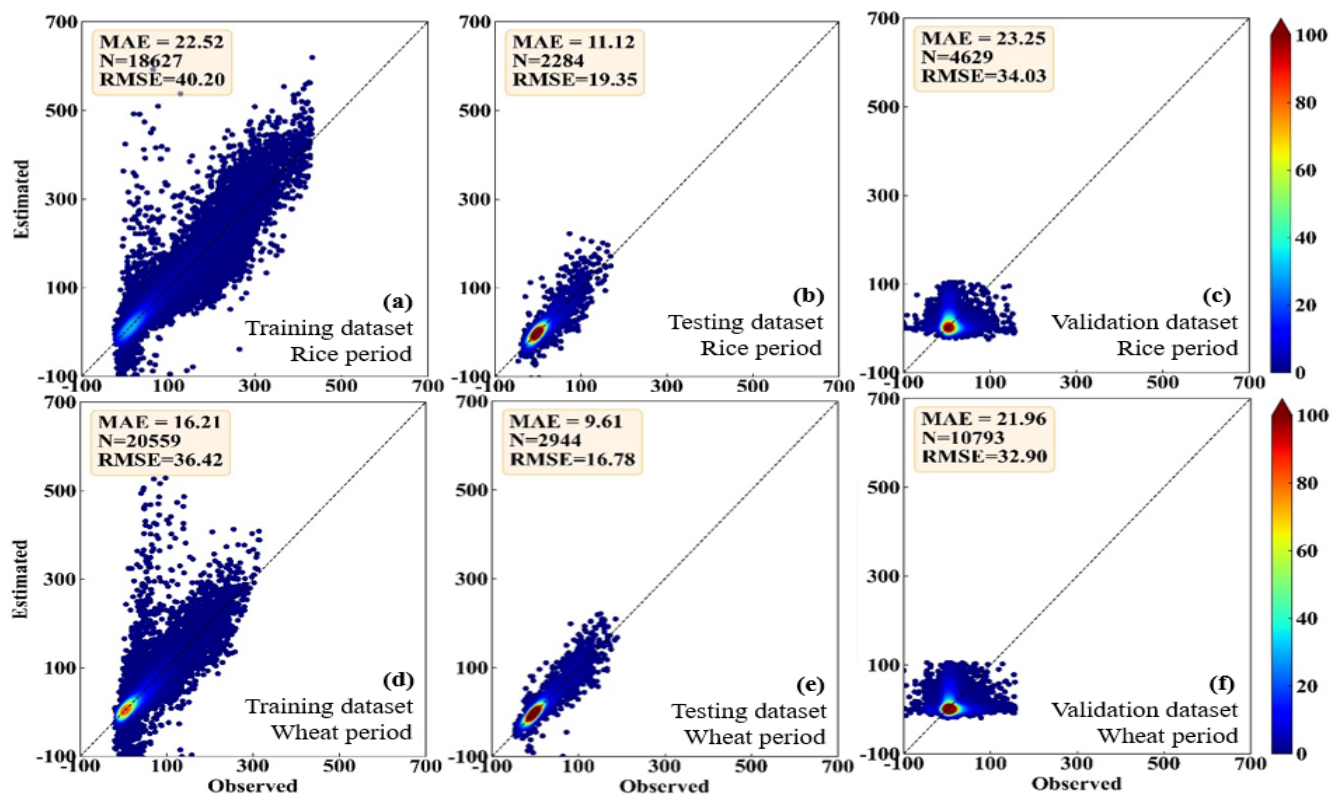


Figure 6. Same as Figure 5, but for LE.

157
 158
 159
 160

161 3.3 Examination of Input Combinations

162 Meteorological elements may occasionally be unavailable due to the failure of sensors so the 5-variable input combination
 163 derived in Section 3.2 is not always applicable. Therefore, examination of other alternative input combinations is important to
 164 have substitute choices for data gap-filling when the 5-variable input combination is unavailable. In this subsection, we
 165 investigated the RF model's performance under the situation of lacking one element in the 5-variable input combination, i.e.,
 166 we tested the 4-variable input combinations of (WS, T, RH, P), (Rn, T, RH, P), (Rn, WS, RH, P), (Rn, WS, T, P), and (Rn,
 167 WS, T, RH), by removing Rn, WS, T, RH, and P from the 5-variable input combination, respectively. The MAEs and RMSEs
 168 for these combinations are shown in Table 1, and it demonstrates that the RF model's accuracy may either increase or decrease
 169 as a result of the removal of a meteorological element during the training phase. For instance, it was found that the model's
 170 performance greatly improved once RH was eliminated from the input combination, with the MAE and RMSE of H decreasing
 171 from 6.48 and 11.94 Wm^{-2} to 5.66 and 11.06 Wm^{-2} , respectively, and LE from 19.1 and 39.39 Wm^{-2} to 17.74 and 35.27 Wm^{-2} .
 172 The results suggested that RH at a single level was not well correlated to the fluxes as shown in Section 3.1, because the



173 one-level RH was strongly affected by the irrigation activity which was an external factor of the weather system. As a result,
 174 RF model performance was enhanced when the irrelevant variable (i.e., RH) was removed from the input list. The same
 175 condition also happened to the removal of WS, as could be seen from Section 3.1, WS showed small correlations with the
 176 fluxes. WS over this site was rather small, and frequently below 2 m s^{-1} , and under this light wind condition, the fluxes were
 177 mostly driven by the buoyancy rather than the wind shear. Figure 7 presents the MAE variation percentage of the 4-variable
 178 input combinations from the 5-variable input combination. After RH was removed from the input list, the RF model showed
 179 favorable performance for both H and LE, as shown in Figure 7, with MAE improvements of 12.65 and 7.12%, respectively.
 180 Notably, the removal of Rn from the input combination resulted in a considerable decline in the RF model's performances,
 181 with MAE degradation percentage values reaching 16.20% and 10.73%, respectively. This outcome makes sense since Rn is
 182 highly associated with H and LE; hence, performance will be declined if Rn is left out of the input training dataset. As a
 183 consequence, our findings demonstrated that choosing strongly associated components could greatly increase the gap-filling
 184 accuracy. According to our findings, the best input combination is (Rn, WS, T, P).

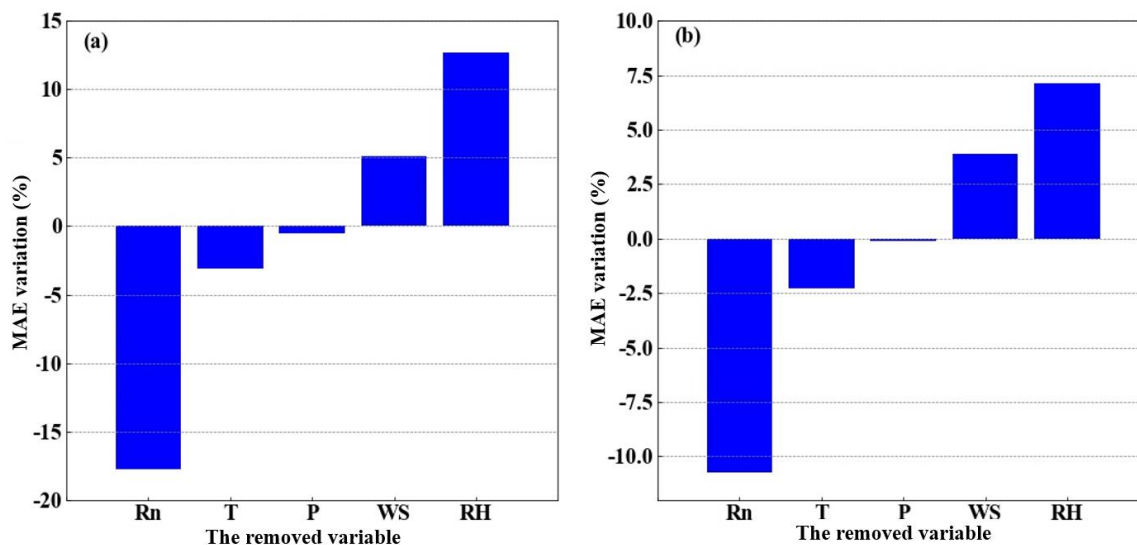
185

186 **Table 1. The MAEs and RMSEs of the RF-estimated heat fluxes for the 4-variable input combinations, and the corresponding**
 187 **changes from the 5-variable input combination.**

188

| Factors Included | Factors Eliminated | | MAE (change) | RMSE (change) |
|----------------------|--------------------|----|---------------|---------------|
| WS, T, RH, P | Rn | H | 7.63 (+1.15) | 10.72 (-1.22) |
| | | LE | 21.15 (+2.05) | 39.38 (-4.62) |
| Rn, T, RH, P | WS | H | 6.15 (-0.33) | 11.42 (-0.52) |
| | | LE | 18.36 (-0.74) | 36.13 (-2.34) |
| Rn, WS, RH, P | T | H | 6.68 (+0.20) | 11.48 (-0.46) |
| | | LE | 19.54 (+0.44) | 38.54 (-1.46) |
| Rn, WS, T, P | RH | H | 5.66 (-0.82) | 11.06 (-0.88) |
| | | LE | 17.74 (-1.36) | 35.27 (-4.12) |
| Rn, WS, T, RH | P | H | 6.49 (+0.03) | 11.77 (-0.17) |
| | | LE | 19.12 (+0.02) | 38.13 (-1.07) |

189



190
191

192 **Figure 7. The MAE percentage variation after changing the 5-variable input combinations to the 4-variable input combinations, a)**
193 **for H, and b) for LE, respectively. The x-axis labels indicate the removed variables.**

194

195 It should be noted that other variables that might have an impact on the H and LE were not investigated here. For example,
196 given that our research site was over farmland and plants were growing, knowledge of the variations of the leaf area index
197 (LAI) and inclusion of it to the training dataset should also be useful to increase the accuracy of the RF model in H and LE
198 gap-filling. The monsoonal climate here also incurred considerable precipitation variations, which might as well potentially
199 contribute to the RF model accuracy improvement. However, due to the lack of LAI and precipitation observations, the
200 inclusion of the two variables into the RF model training dataset was not applicable in this study. Additionally, as shown above,
201 more variables would bring a higher observation demand, and lead to more complexity and potentially decreased results, such
202 as the adding variable of RH.

203

204 3.4 Comparison with other four ML methods

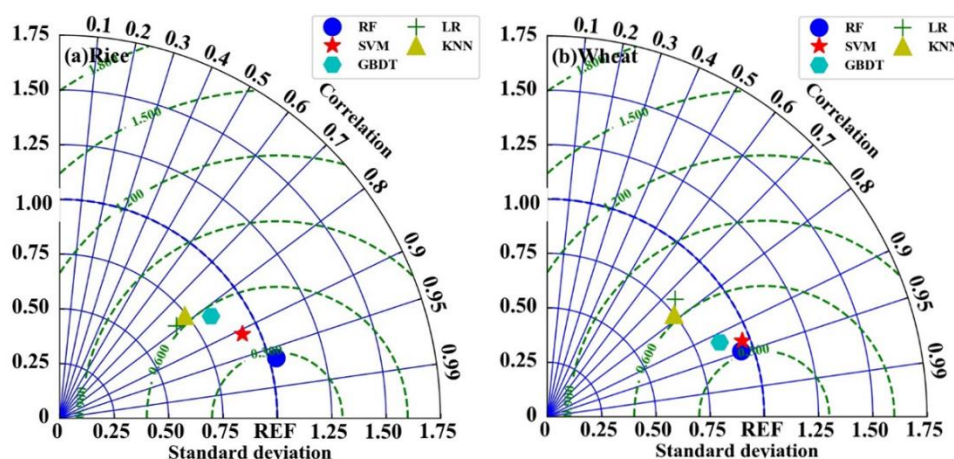
205 3.4.1 Comparison in H estimation

206

207 To further investigate the reliability of the RF model, we used a Taylor diagram to compare its performance in H estimation
208 with other four ML models: linear regression (LR), k-nearest neighbor (KNN), support vector machine (SVM), and gradient
209 boosting decision tree (GBDT). All the models were optimized with the same technique described above for the RF model.
210 The results are shown in Figure 8. The EC measurements were used as the benchmark. It can be seen that the RF model
211 generally outperforms the other four models, with the standard deviation (σ_n) and correlation values of 1.05 and 0.98 during



212 the period of rice planting, and 0.96 and 0.95 during the period of wheat planting, respectively. The SVM model is the second
 213 most accurate model, with the σ_n and correlation of 0.92 and 0.98 during the period of rice planting, and 0.91 and 0.93 during
 214 the period of wheat planting, respectively. The LR model performs the worst, with the σ_n and correlation of 0.60 and 0.76
 215 during the period of rice planting, and 0.80 and 0.72 during the period of wheat planting, respectively. The accuracy of KNN
 216 and the GBDT models is in between the above-discussed models, and the σ_n and correlation during the rice and wheat period
 217 for KNN are 0.68 and 0.73, and 0.77 and 0.82; and for GBDT are 0.79 and 0.80, and 0.81 and 0.9, respectively.
 218



219
 220

221 **Figure 8. Taylor diagram visualizing the performances of the five models for estimating H in the period of a) rice and b) wheat.**

222

223 3.4.2 Comparison in LE estimation

224

225 Figure 9 illustrates a comparison of the estimated LE by all the five models during the period of rice and wheat planting. The
 226 results are similar to those in the H estimation, and the RF model is found to perform better than the other four models, with
 227 the σ_n and correlation values of 0.95 and 0.97 during the period of rice planting, and 0.97 and 0.96 during the period of wheat
 228 planting, respectively. Nonetheless, the KNN model performs the worse for LE estimating and has the σ_n and correlation
 229 values of 0.68 and 0.82 during the period of rice planting, and 0.62 and 0.79 during the period of wheat planting, respectively.
 230 Overall, as shown by the Taylor diagram of Figures 8 and 9, in this study the RF model has the best accuracy in either H or
 231 LE estimation for data gap-filling.

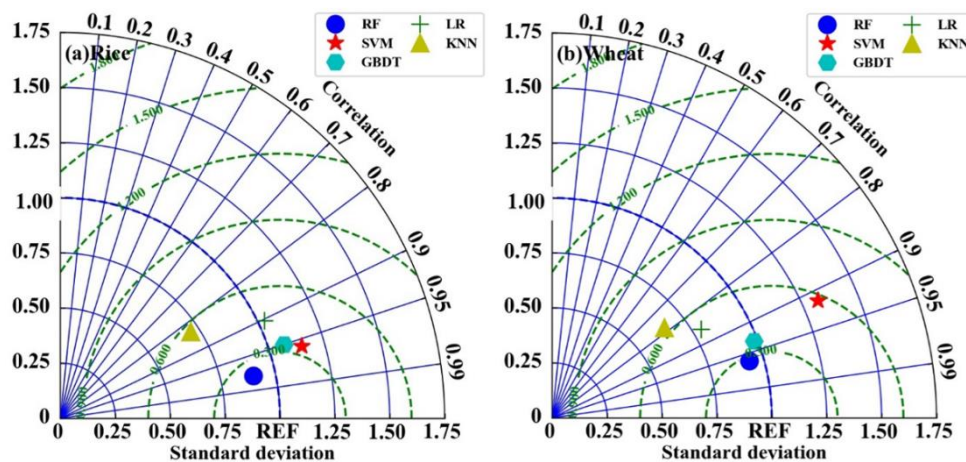


Figure 9. Same as Figure 8, but for LE

232
 233
 234
 235

236 4 Summary and Conclusions

237 To assess the RF model's capacity for gap-filling the sensible and latent heat flux measurements over rice-wheat rotation
 238 croplands, 90% of the total observation data gathered at Shouxian were utilized for training and testing, and the remaining 10%
 239 for independent validation. Our findings demonstrate that R_n is the most important variable in regulating H and LE , and it
 240 accounts for 78% and 76% of the total variable significance in the RF model construction for H and LE calculation, respectively.
 241 The least important variables are WS and P , and their total variable significances are 2% and 0.6%, respectively. During the
 242 periods of rice and wheat planting, the RF model with a 5-variable input combination shows reliable performance, with MAE
 243 values of 5.88 Wm^{-2} and 20.97 Wm^{-2} , and RMSE values of 10.67 Wm^{-2} and 29.46 Wm^{-2} , respectively. However, further
 244 analysis of the RF model with 4-variable input combinations indicates that the performance of the model is improved when
 245 RH is removed from the input list, and the MAE decreases by 12.65% and 7.12% for H and LE , respectively. Nonetheless, the
 246 4- variable input combination without R_n causes an increase in the MAE of the model, by 16.20% and 10.73% for H and LE ,
 247 respectively. Therefore, the best input combination found in this study for heat fluxes gap-filling is (R_n , WS , T , P). Statistical
 248 comparison of RF and other four typical ML models (LR, KNN, SVM, and GBDT) by Tylor diagram further shows that RF is
 249 the most accurate, with the σ_n and correlation values of 0.95 and 0.97 during the period of rice planting, and 0.97 and 0.96
 250 during the period of wheat planting, respectively. While the LR and KNN models perform the worst for H and LE gap-filling,
 251 respectively, according to the statistical metrics of the Tylor diagram.

252

253 This study is based on only the data collected over rice-wheat-rotation croplands, but the method presented above to find a
 254 reliable heat fluxes gap-filling ML model can also be used over the underlying surface of other types and in other climate



255 zones. It should be noted that over different types of the underlying surface and climates, the variable significances can vary
256 and a careful check of the input combinations is needed. For example, over polar oceans with strong winds, R_n probably is not
257 the most important driving factor, while the winds which cause mostly the turbulence may take the first place. On the other
258 hand, over areas without human irrigation activity, RH will possibly be strongly related to the latent heat flux, and hence the
259 inclusion of it into the input list may increase the ML model performance. Besides the examination of the input combinations,
260 the choice of an ML model and the method to optimize its parameters are also important.

261

262 Overall, this study shows the potential to use the RF model to produce trustworthy gap-filling data of H and LE over rice–
263 wheat-rotation croplands, and the ML methods are suggested to be used to derive the fluxes' estimations when direct EC
264 observations are not available.

265

266 References

- 267 Alavi, N., Warland, J.S., Berg, A.A.: Filling gaps in evapotranspiration measurements for water budget studies: Evaluation of
268 a Kalman filtering approach, *J. Agric. For. Meteorol.*, 141 (1), 57–66, <https://doi.org/10.1016/j.agrformet.2006.09.011>,
269 2006.
- 270 Anapalli, S.S.; Fisher, D.K.; Reddy, K.N.; Krutz, J.L.; Pinnamaneni, S.R.; Sui, R.: Quantifying water and CO₂ fluxes and water
271 use efficiencies across irrigated C3 and C4 crops in a humid climate, *J. Sci. Total Environ.*, 663, 338–350,
272 <https://doi.org/10.1016/j.scitotenv.2018.12.471>, 2018.
- 273 Baareh, A.K.; Elsayad, A.; Al-Dhaifallah, M.: Recognition of splice-junction genetic sequences using random forest and
274 Bayesian optimization, *J. Multimed. Tools Appl.*, 80, 30505–30522, <https://doi.org/10.1007/s11042-021-10944-7>, 2021.
- 275 Belgiu, M.; Dragut, L.: Random forest in remote sensing: A review of applications and future directions, *Isprs J. Photogramm.*
276 *J. Remote Sensing.*, 114, 24–31, <https://doi.org/10.1016/j.isprsjprs.2016.01.011>, 2016.
- 277 Beringer, J., McHugh, I., Hutley, L. B., Isaac, P., and Kljun, N.: Technical note: Dynamic INtegrated Gap-filling and
278 partitioning for OzFlux (DINGO), *J. Biogeosciences.*, 14, 1457–1460, <https://doi.org/10.5194/bg-14-1457-2017>, 2017.
- 279 Best, M. J., M. Pryor, D. B. Clark, G. G. Rooney, et al.: The Joint UK Land Environment Simulator (JULES), model description
280 - Part 1: Energy and water fluxes, *J. Geosci. Model Dev.*, 4, 677–699, <https://doi.org/10.5194/gmd-4-677-2011>, 2011.
- 281 Bianco, M.J.; Gerstoft, P.; Traer, J.; Ozanich, E.; Roch, M.A.; Gannot, S.; Deledalle, C.-A.: Machine learning in acoustics:
282 Theory and applications, *J. Acoust. Soc. Am.*, 146, 3590–3628, <https://doi.org/10.1121/1.5133944>, 2019.
- 283 Breiman, L.: Random Forests, *J. Mach. Learn.*, 45, 5–32, <https://doi.org/10.1023/A:1010933404324>, 2001.
- 284 Cai, J.C.; Xu, K.; Zhu, Y.H.; Hu, F.; Li, L.H.: Prediction and analysis of net ecosystem carbon exchange based on gradient
285 boosting regression and random forest, *J. Appl. Energy.*, 262, 114566, <https://doi.org/10.1016/j.apenergy.2020.114566>,
286 2020.



- 287 Duan, Z.; Grimmond, C.; Gao, C.Y.; Sun, T.; Liu, C.; Wang, L.; Li, Y.; Gao, Z.: Seasonal and interannual variations in the
288 surface energy fluxes of a rice–wheat rotation in Eastern China, *J. Appl. Meteorol. Climatol.*, 60, 877–891,
289 <https://doi.org/10.1175/JAMC-D-20-0233.1>, 2021.
- 290 Duan, Z.; Yang, Y.; Wang, L.; Liu, C.; Fan, S.; Chen, C.; Tong, Y.; Lin, X.; Gao, Z.: Temporal characteristics of carbon
291 dioxide and ozone over a rural-cropland area in the Yangtze River Delta of eastern China, *J. Sci. Total Environ.*, 757,
292 e143750, <https://doi.org/10.1016/j.scitotenv.2020.143750>, 2021.
- 293 Falge, E.; Baldocchi, D.; Olson, R.; Anthoni, P.; Aubinet, M.; Bernhofer, C.; Burba, G.; Ceulemans, R.; Clement, R.; Dolman,
294 H.: Gap filling strategies for defensible annual sums of net ecosystem exchange, *J. Agric. For. Meteorol.*, 107, 43–69,
295 [https://doi.org/10.1016/S0168-1923\(00\)00225-2](https://doi.org/10.1016/S0168-1923(00)00225-2), 2001.
- 296 Folt ́nov ́ L.; Fischer, M.; McGloin, R.P.: Recommendations for gap-filling eddy covariance latent heat flux measurements
297 using marginal distribution sampling, *J. Theor. Appl. Climatol.*, 139, 677–688, <https://doi.org/10.1007/s00704-019-02975-w>, 2020.
- 299 Frazier, P.I.: A Tutorial on Bayesian Optimization, arXiv 2018, <https://doi.org/10.48550/arXiv.1807.02811>, 2018.
- 300 Gao, Z. Q., L. G. Bian, and X. J. Zhou.: Measurements of turbulent transfer in the near-surface layer over a rice paddy in China,
301 *J. Geophys. Res.*, 108(D13), 4387–4387, <https://doi.org/10.1029/2002JD002779>, 2003.
- 302 Garratt, J. R.: The atmospheric boundary layer. Cambridge Atmospheric and Space Science Series, Cambridge University
303 Press, 316, <https://doi.org/10.1017/CBO9781316117422>, 2015.
- 304 Hui, D.; Wan, S.; Su, B.; Katul, G.; Monson, R.; Luo, Y.: Gap-filling missing data in eddy covariance measurements using
305 multiple imputation (MI) for annual estimations, *J. Agric. For. Meteorol.*, 121, 93–111, [https://doi.org/10.1016/S0168-1923\(03\)00158-8](https://doi.org/10.1016/S0168-1923(03)00158-8), 2004.
- 307 Isaac, P., Cleverly, J., McHugh, I., Van Gorsel, E., Ewenz, C., and Beringer, J.: OzFlux data: Network integration from
308 collection to curation, *J. Biogeosciences*, 14, 2903–2928, <https://doi.org/10.5194/bg-14-2903-2017>, 2017.
- 309 Jiang, L.; Zhang, B.; Han, S.; Chen, H.; Wei, Z.: Upscaling evapotranspiration from the instantaneous to the daily time scale:
310 Assessing six methods including an optimized coefficient based on worldwide eddy covariance flux network, *J. Hydrol.*,
311 596, 126135, <https://doi.org/10.1016/j.jhydrol.2021.126135>, 2021.
- 312 Kepert, J.: Choosing a boundary layer parameterization for tropical cyclone modelling, *J. Mon. Wea. Rev.* [serial online].,
313 140(5), 1427–1445, DOI: <https://doi.org/10.1175/MWR-D-11-00217.1>, 2012.
- 314 Khan, M.S.; Jeon, S.B.; Jeong, M.H.: Gap-Filling Eddy Covariance Latent Heat Flux: Inter-Comparison of Four Machine
315 Learning Model Predictions and Uncertainties in Forest Ecosystem, *J. Remote Sens.*, 13, 4976.
316 <https://doi.org/10.3390/rs13244976>, 2021.
- 317 Khan, M.S.; Liaqat, U.W.; Baik, J.; Choi, M.: Stand-alone uncertainty characterization of GLEAM, GLDAS and MOD16
318 evapotranspiration products using an extended triple collocation approach, *J. Agric. For. Meteorol.*, 252, 256–268,
319 <https://doi.org/10.1016/j.agrformet.2018.01.022>, 2018.



- 320 Kim, Y.; Johnson, M.S.; Knox, S.H.; Black, T.A.; Dalmagro, H.J.; Kang, M.; Kim, J.; Baldocchi, D.: Gap-filling approaches
321 for eddy covariance methane fluxes: A comparison of three machine learning algorithms and a traditional method with
322 principal component analysis, *J. Glob. Chang. Biol.*, 26, 1499–1518, <https://doi.org/10.1111/gcb.14845>, 2020.
- 323 Kunwor, S., Starr, G., Loescher, H. W., and Staudhammer, C. L.: Preserving the variance in imputed eddy covariance
324 measurements: Alternative methods for defensible gap filling, *J. Agr. Forest Meteorol.*, 232, 635–649,
325 <https://doi.org/10.1016/j.agrformet.2016.10.018>, 2017.
- 326 Li, X., Z. Gao, Y. Li, and B. Tong.: Comparison of sensible heat fluxes measured by a large aperture scintillometer and eddy
327 covariance system over a heterogeneous farmland in East China, *J. Atmosphere.*, 8, 101, [https://doi.org/10.3390/
328 atmos8060101](https://doi.org/10.3390/atmos8060101), 2017.
- 329 Liu, J.; Zuo, Y.; Wang, N.; Yuan, F.; Zhu, X.; Zhang, L.; Zhang, J.; Sun, Y.; Guo, Z.; Guo, Y.; et al.: Comparative Analysis
330 of Two Machine Learning Algorithms in Predicting Site-Level Net Ecosystem Exchange in Major Biomes, *J. Remote
331 Sens.*, 13, 2242, <https://doi.org/10.3390/rs13122242>, 2021.
- 332 McCandless, T., Gagne, D. J., Kosović, B., Haupt, S. E., Yang, B., Becker, C., & Schreck, J. (2022). Machine Learning for
333 Improving Surface-Layer-Flux Estimates. *Boundary-Layer Meteorology*, 185(2), 199-228.
- 334 Moffat, A. M., Papale, D., Reichstein, M., Hollinger, D. Y., Richardson, A. D., Barr, A. G., Beckstein, C., Braswell, B. H.,
335 Churkin G., Desai, A. R., Falge, E., Gove, J. H., Heimann, M., Hui, D., Jarvis, A. J., Kattge, J., Noormets, A., and Stauch,
336 V. J.: Comprehensive comparison of gap-filling techniques for eddy covariance net carbon fluxes, *J. Agr. Forest Meteorol.*,
337 147, 209–232, <https://doi.org/10.1016/j.agrformet.2007.08.011>, 2007.
- 338 Moncrieff, J.; Clement, R.; Finnigan, J.; Meyers, T.: Averaging, Detrending, and Filtering of Eddy Covariance Time Series.
339 In *Handbook of Micrometeorology: A Guide for Surface Flux Measurement and Analysis*, The Netherlands, pp., 7–31,
340 https://doi.org/10.1007/1-4020-2265-4_2, 2006.
- 341 Monin, A. S., & Obukhov, A. M. (1954). Basic laws of turbulent mixing in the surface layer of the atmosphere. *Contrib.*
342 *Geophys. Inst. Acad. Sci. USSR*, 151(163), e187.
- 343 Nisa, Z.; Khan, M.S.; Govind, A.; Marchetti, M.; Lasserre, B.; Magliulo, E.; Manco, A.: Evaluation of SEBS, METRIC-
344 EEFlux, and QWaterModel Actual Evapotranspiration for a Mediterranean Cropping System in Southern Italy, *J. Remote
345 Sens.*, 13, 4976 18 of 19, <https://doi.org/10.3390/agronomy11020345>, 2021.
- 346 Papale, D.; Reichstein, M.; Aubinet, M.; Canfora, E.; Bernhofer, C.; Kutsch, W.; Longdoz, B.; Rambal, S.; Valentini, R.;
347 Vesala, T.; et al.: Towards a standardized processing of Net Ecosystem Exchange measured with eddy covariance
348 technique: Algorithms and uncertainty estimation, *J. Biogeosciences.*, 3, 571–583, <https://doi.org/10.5194/bg-3-571-2006>,
349 2006.
- 350 Reichstein, M.; Falge, E.; Baldocchi, D.; Papale, D.; Aubinet, M.; Berbigier, P.; Bernhofer, C.; Buchmann, N.; Gilmanov, T.;
351 Granier, A.; et al.: On the separation of net ecosystem exchange into assimilation and ecosystem respiration: Review and
352 improved algorithm, *J. Glob. Change Biol.*, 11, 1424–1439, <https://doi.org/10.1111/j.1365-2486.2005.001002.x>, 2005.



- 353 Richard, A.; Fine, L.; Rozenstein, O.; Tanny, J.; Geist, M.; Pradalier, C.: Filling Gaps in Micro-Meteorological Data,
354 Switzerland, https://doi.org/10.1007/978-3-030-67670-4_7, 2020.
- 355 Stauch, V.J.; Jarvis, A.J.: A semi-parametric gap-filling model for eddy covariance CO₂ flux time series data, *J. Glob. Chang.*
356 *Biol.*, 12, 1707–1716, <https://doi.org/10.1111/j.1365-2486.2006.01227.x>, 2006.
- 357 Vitale, D.; Bilancia, M.; Papale, D.: A multiple imputation strategy for eddy covariance data, *J. Environ. Inform.*, 34, 68–87,
358 <https://doi.org/10.3808/jei.201800391>, 2018.
- 359 Wang, L.; Wu, B.; Elnashar, A.; Zeng, H.; Zhu, W.; Yan, N.: Synthesizing a Regional Territorial Evapotranspiration Dataset
360 for Northern China, *J. Remote Sens.*, 13, 1076, <https://doi.org/10.3390/rs13061076>, 2021.
- 361 Webb, E.K.; Pearman, G.I.; Leuning, R. Correction of flux measurements for density effects due to heat and water vapor
362 Transfer, *Q. J. R. Meteorol. Soc.*, 106, 85–100, <https://doi.org/10.1002/qj.49710644707>, 1980.
- 363 Wilson, K.B.; Hanson, P.J.; Mulholland, P.J.; Baldocchi, D.D.; Wullschleger, S.D.: A comparison of methods for determining
364 forest evapotranspiration and its components: Sap-flow, soil water budget, eddy covariance and catchment water balance,
365 *J. Agric. For. Meteorol.*, 106, 153–168, [https://doi.org/10.1016/S0168-1923\(00\)00199-4](https://doi.org/10.1016/S0168-1923(00)00199-4), 2001.
- 366 Wutzler, T., Lucas-Moffat, A., Migliavacca, M., Knauer, J., Sickel, K., Sigut, L., Reichstein, M.: Basic and extensible post-
367 processing of eddy covariance flux data with REddyProc, *J. Biogeosciences.*, 15 (16): 5015–5030,
368 <https://doi.org/10.5194/bg-15-5015-2018>, 2018.
- 369 Yu, T.C.; Fang, S.Y.; Chiu, H.S.; Hu, K.S.; Tai, P.H.Y.; Shen, C.C.F.; Sheng, H.: Pin accessibility prediction and optimization
370 with deep learning-based pin pattern recognition, *J. IEEE Trans. Comput.-Aided Des. Integr. Circuits Syst.*, 40, 2345–
371 2356, <https://doi.org/10.1145/3316781.3317882>, 2019.